NOLTA, IEICE

Paper

Turing patterns in the simplest MCNN

Maide Bucolo [1], *Arturo Buscarino* [1,2 a)], *Claudia Corradino* [1], *Luigi Fortuna* [1,2], *and Mattia Frasca* [1,2]

[1] *Dipartimento di Ingegneria Elettrica Elettronica e Informatica, University of Catania, Italy*

[2] *CNR-IASI, Italian National Research Council - Institute for Systems Analysis and Computer Science "A. Ruberti", Rome, Italy*

[a)] *arturo.buscarino@unict.it*

Received January 10, 2019; Revised April 19, 2019; Published October 1, 2019

Abstract: Complex patterns can be often retrieved in spatially-extended systems formed by coupled nonlinear dynamical units. In particular, Turing patterns have been extensively studied investigating mathematical models related to different contexts, such as chemistry, physics, biology, and also mechanics and electronics. In this paper, we focus on the emergence of Turing patterns in a circuit architecture formed by coupled units in which a memrsitive element is considered. Furthermore, the unit is formed by only two elements, namely a capacitor and a memristor. The analytical conditions for which Turing patterns can be obtained in the proposed architecture are discussed in order to inform the design of the circuit parameters. Moreover, the characterization of the different types of patterns is performed with respect to the strength of the diffusion occurring between the units. Finally, it is worth to note that the proposed architecture can be considered as the simplest electronic circuit able to undergo Turing instability and give rise to pattern formation.

Key Words: memristor, Cellular Nonlinear Networks, Turing patterns, cross-diffusion

1. Introduction

Since the seminal work on morphogenesis in biological organisms proposed by Alan Turing [1], many efforts have been devoted to fully understand mechanisms dealing with pattern formation in areas such as biology and chemistry. Phenomena leading to pattern formation in spatially-extended systems have been also investigated in fields far from biology, namely mechanics [2], electronics [3] and thermodynamics [4]. These studies are based on the use of models belonging to a class of nonlinear differential equations, known as reaction-diffusion models, which are adopted to mimic the dynamics of spatially-extended systems where a competitive inhibition-activation effect occurs. The spatial extension of such systems involves a suitable discretization of the active medium in *cells*, i.e. basic units of the reaction-diffusion model, usually described as second-order systems, in which state variables represent the two concentrations of morphogenes [1]. Diffusion processes occur in the presence of a gradient in the morphogene concentrations, in particular a self-diffusion occurs if one morphogene induces a flux of the same morphogene, otherwise when different chemical species are actually diffusing, a cross-diffusion process occurs. Although cross-diffusion is usually neglected, in many natural pro-

Nonlinear Theory and Its Applications, IEICE, vol. 10, no. 4, pp. 390–398 DOI: 10.1587/nolta.10.390

cesses, such as chemotaxis, ecology and social systems, it is shown to play a central role [5]. Recently, evidence of Turing pattern formation has been presented in a spatially-extended electronic system in which cross-diffusion is considered [6].

In order to implement the circuit architecture considered in this paper, the Cellular Nonlinear Networks (CNNs) paradigm has been adopted. This choice has been widely explored in the past to study spatio-temporal phenomena, including Turing patterns and autowaves formation. In fact, CNNs are perfectly suited to fit the structure of reaction-diffusion systems, since they can be used to map partial differential equations [3].

In pattern formation, the presence of nonlinear elements is fundamental. Therefore, in this paper we considered one of the most interesting nonlinear device, the memristor [7, 8]. Theorized in 1971 [9], the first actual memristor has been implemented after three decades at the Hewlett-Packard laboratories [7]. It is a two-terminal electronic device displaying a functional relationship between the time integral of the current through it and that of the voltage across its terminals. Different models can be retrieved for memristive devices, either based on the physics of the component, or on the representation of the functional relationship between flux and charge. Furthermore, its nonlinearity is modeled by means of piece-wise linear [10] or more sophisticated functions [11, 12].

As shown in [6, 13, 14], memristive CNNs (MCNN) made of memristor-based basic cells may be adopted for the investigation of spatio-temporal phenomena such as autowaves formation and Turing patterns. In these works, a basic cell with three circuit elements (a linear passive inductor, a linear passive capacitor and a nonlinear active memristor) was considered for the reaction-diffusion MCNN. In this paper, we propose a new MCNN model consisting in a two-dimensional array of cells made by only two components: a linear passive capacitor and a nonlinear active memristor. Thus, the proposed circuit not only reduces the number of circuit elements required, but it represents the simplest possible cell able to generate Turing patterns. In addition, quite counterintuitively, the adoption of a simplified cell also leads to a simplification of the coupling mechanism: in accordance with real cases described in [5] our results in fact point out that only cross-diffusion of a single species towards the other is needed for pattern formation.

The remainder of the paper is organized as follows: in Section 2 the MCNN is described; in Section 3 the conditions for the emergence of Turing patterns are determined for the proposed MCNN system; in Section 4 numerical results are presented showing the different types of Turing patterns that can be observed in the proposed MCNN; in Section 5 the conclusions are reported.

2. The memristive Cellular Nonlinear Network

The MCNN discussed in the following represents an active medium discretized in a lattice of $N \times N$ basic cells. At first the basic cell will be described with the aim of deriving the set of equations governing the dynamical behavior of the whole structure.

The basic cell is the simple electronic circuit reported in Fig. 1. It is composed by the parallel of two basic components: a capacitor, which is linear and passive, and a memristor. As in [15], the memristor is actually a memristive system, whose model is defined by the following equations:

$$\begin{aligned} i_M &= M(\phi)v_M = \beta(\phi^2 - 1)v_M \\ \dot{\phi} &= f_M(\phi, v_M) = v_M - \alpha\phi - v_M\phi \end{aligned} \tag{1}$$

where v_M and i_M are the voltage and the current, respectively, associated to the memristive sys-

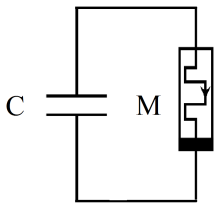

Fig. 1. Schematic representation of two memristor-based circuits: memristor-capacitor circuit.

tem, ϕ is the internal state, i.e. the flux, $f_M(\phi, v_M)$ is the internal state function, and $M(\phi)$ is the memductance of the memristive system. Furthermore, α and β are constant parameters.

Applying the standard Kirchhoff laws and the model in Eqs. (1) to the circuit in Fig. 1, the following equations can be derived:

$$\begin{aligned} C\dot{v} &= -\beta(\phi^2 - 1)v \\ \dot{\phi} &= v - \alpha\phi - v\phi \end{aligned} \tag{2}$$

where v is the voltages across both the capacitor C and the memristor M, and ϕ is the flux associated with the memristor. Introducing the dimensionless variables $x = v$, $y = \phi$ and the parameter $\gamma = \frac{1}{C}$, Eqs. (2) can be rewritten as:

$$\begin{aligned} \dot{x} &= -\gamma\beta(y^2 - 1)x \\ \dot{y} &= x - \alpha y - xy \end{aligned} \tag{3}$$

The model describing the $N \times N$ MCNN is obtained by considering the circuit equations (3) as the model governing each cell of the grid and introducing a diffusive coupling which locally connects it with its four nearest neighbors as:

$$\begin{aligned} \dot{x}_{i,j} &= -\gamma\beta(y_{i,j}^2 - 1)x_{i,j} + D_{11}(x_{i-1,j} + x_{i+1,j} + x_{i,j-1} + x_{i,j+1} - 4x_{i,j}) \\ &\quad + D_{12}(y_{i-1,j} + y_{i+1,j} + y_{i,j-1} + y_{i,j+1} - 4y_{i,j}) \\ \dot{y}_{i,j} &= x_{i,j} - \alpha y_{i,j} - x_{i,j}y_{i,j} + D_{21}(x_{i-1,j} + x_{i+1,j} + x_{i,j-1} + x_{i,j+1} - 4x_{i,j}) \\ &\quad + D_{22}(y_{i-1,j} + y_{i+1,j} + y_{i,j-1} + y_{i,j+1} - 4y_{i,j}) \end{aligned} \tag{4}$$

where i, j represent the indices of the row and the column, D_{11} and D_{22} are the self-diffusion coefficients, while D_{12} and D_{21} are the cross-diffusion coefficients. The set of dynamical equations (4) represents a reaction-diffusion system in which a general form of diffusion takes place, i.e. a process which includes both self- and cross-diffusion among variables.

We now rewrite Eqs. (4) in compact form by defining $f(x, y) = -\gamma\beta(y^2 - 1)x$ and $g(x, y) = x - \alpha y - xy$, and adopting the following notation for the two-dimensional discrete Laplacian:

$$\begin{aligned} \nabla^2 x_{i,j} &= x_{i+1,j} + x_{i,j-1} + x_{i,j+1} - 4x_{i,j} \\ \nabla^2 y_{i,j} &= y_{i+1,j} + y_{i,j-1} + y_{i,j+1} - 4y_{i,j} \end{aligned} \tag{5}$$

In this way, system (4) is written as

$$\begin{aligned} \dot{x}_{i,j} &= f(x_{i,j}, y_{i,j}) + D_{11}\nabla^2 x_{i,j} + D_{12}\nabla^2 y_{i,j} \\ \dot{y}_{i,j} &= g(x_{i,j}, y_{i,j}) + D_{21}\nabla^2 x_{i,j} + D_{22}\nabla^2 y_{i,j} \end{aligned} \tag{6}$$

In addition, in the following the partial derivatives of the functions $f(x, y)$ and $g(x, y)$ will be denoted by $f_x = \frac{\partial f}{\partial x}$, $f_y = \frac{\partial f}{\partial y}$, $g_x = \frac{\partial g}{\partial x}$ and $g_y = \frac{\partial g}{\partial y}$.

3. Turing conditions

The reaction-diffusion model in Eqs. (6) may exhibit Turing patterns, that is diffusion-driven instability, when the equilibrium point of the isolated cell is stable but it is driven to instability when the diffusion process takes place. This principle can be translated into mathematical conditions by first considering the cell as isolated, linearizing the dynamics around its equilibrium and studying the stability of its equilibrium point through the analysis of the Jacobian matrix. A first set of conditions is obtained by imposing that the equilibrium point is stable. Then, the effect of the diffusion is considered through a technique based on the evaluation of the spatial eigenvalues, which allows to consider the effect of the coupling. The stability of the system is then investigated deriving the conditions on the parameters such that the equilibrium point becomes unstable [16]. In this section, this approach is applied to the MCNN in Eqs. (6) in order to derive the conditions in the parameter space leading to the emergence of Turing patterns.

The isolated cell described by Eqs. (3) admits two equilibrium points, one located at the origin $Q_0 = (0, 0)$, and the other in $Q_1 = (-\frac{\alpha}{2}, -1)$. We focus on Q_1, since for Q_0 two mutually excluding

conditions arise. The stability of Q_1 is, therefore, studied through the eigenvalues of Jacobian matrix A, evaluated around Q_1:

$$\mathrm{A} = \left[\begin{array}{cc} f_x & f_y \\ g_x & g_y \end{array} \right]_{(x,y)=(-\frac{\alpha}{2},-1)} = \left[\begin{array}{cc} -\gamma\beta(y^2-1)x & -2\gamma\beta yx \\ 1-y & -\alpha-x \end{array} \right]_{(x,y)=(-\frac{\alpha}{2},-1)} = \left[\begin{array}{cc} 0 & -\gamma\alpha\beta \\ 2 & -\frac{\alpha}{2} \end{array} \right], \quad (7)$$

Setting $\gamma = 1$, and indicating with

$$\begin{array}{l} \mathrm{tr(A)} = (f_x + g_y)|_{(x,y)=(-\frac{\alpha}{2},-1)} = -\frac{\alpha}{2} \\ \det(\mathrm{A}) = (f_x g_y - f_y g_x)|_{(x,y)=(-\frac{\alpha}{2},-1)} = 2\alpha\beta \end{array} \quad (8)$$

the characteristic polynomial of the matrix A takes the following form:

$$\lambda^2 - \mathrm{tr(A)}\lambda + \det(\mathrm{A}) = 0 \quad (9)$$

The equilibrium point Q_1 is, hence, stable if and only if $\mathrm{tr(A)} < 0$ and $\det(\mathrm{A}) > 0$. As a consequence, the first two conditions for Turing patterns are:

$$\begin{array}{ll} -\frac{\alpha}{2} < 0 & (C.1) \\ \alpha\beta > 0 & (C.2) \end{array}$$

Let us consider now the MCNN state equations (6). In order to obtain the conditions on the coupled system, Eqs. (6) are linearized around the equilibrium point Q_1 of the isolated cell [3] obtaining:

$$\begin{array}{l} \dot{\tilde{x}}_{i,j} = f_x \tilde{x}_{i,j} + f_y \tilde{y}_{i,j} + D_{11}\nabla^2 \tilde{x}_{i,j} + D_{12}\nabla^2 \tilde{y}_{i,j} \\ \dot{\tilde{y}}_{i,j} = g_x \tilde{x}_{i,j} + g_y \tilde{y}_{i,j} + D_{21}\nabla^2 \tilde{x}_{i,j} + D_{22}\nabla^2 \tilde{y}_{i,j} \end{array} \quad (10)$$

The properties of (10) are analyzed by the spatial eigenfunction-based decoupling [3]. This approach allows us to study a system of $2N^2$ coupled differential equations as N^2 uncoupled systems of two first-order differential equations. The main idea behind this approach is to find a solution of the MCNN as a weighted sum of N^2 orthonormal space-dependent eigenfunctions $\phi_{N^2}(m,n,i,j)$ associated with the discrete Laplacian operator:

$$\begin{array}{l} \nabla^2 \phi_{N^2}(m,n,i,j) = \phi_{N^2}(m,n,i+1,j) + \phi_{N^2}(m,n,i-1,j) + \phi_{N^2}(m,n,i,j+1) \\ +\phi_{N^2}(m,n,i,j-1) - 4\phi_{N^2}(m,n,i,j) = -k_{mn}^2 \phi_{N^2}(m,n,i,j) \end{array} \quad (11)$$

where k_{mn}^2 are the corresponding spatial eigenvalues and the form of $\phi_{N^2}(m,n,i,j)$ depends on the boundary conditions [3].

If one of the modes k_{mn}^2 is unstable, diffusion-driven instability is induced. To check the occurrence of this condition, the stability of the equilibrium point of the cell in the presence of diffusion is studied with respect to k^2. Hence, in the following equations the index mn will be dropped, thus neglecting which mode becomes unstable. Then, the instability of the MCNN when diffusion is present depends on the following Jacobian matrix:

$$\mathrm{J} = \mathrm{A} - k^2 \mathrm{D} = \left[\begin{array}{cc} -k^2 D_{11} & -\alpha\beta - k^2 D_{12} \\ 2 - k^2 D_{21} & -\frac{\alpha}{2} - k^2 D_{22} \end{array} \right], \quad (12)$$

where k^2 is the spatial eigenvalue, and $\mathrm{D} = \left[\begin{array}{cc} D_{11} & D_{12} \\ D_{21} & D_{22} \end{array} \right]$ is the diffusion coefficients matrix.

The conditions for Turing instability requires that the Jacobian matrix J admits at least an unstable eigenvalue. This implies that $\mathrm{tr(J)} > 0$ or $\det(\mathrm{J}) < 0$. In our case, the trace and the determinant of J are:

$$\begin{array}{l} \mathrm{tr(J)} = -k^2(D_{11}+D_{22}) + \mathrm{tr(A)} = -k^2(D_{11}+D_{22}) - \frac{\alpha}{2} \\ \det(\mathrm{J}) = -(D_{22}f_x + D_{11}f_y - D_{21}g_x - D_{12}f_y)k^2 + \det(D)k^4 + \det(\mathrm{A}) \\ \qquad = (D_{11}D_{22} - D_{12}D_{21})k^4 - (-\frac{\alpha}{2}D_{11} - 2D_{12} + \alpha\beta D_{21})k^2 + 2\alpha\beta \end{array} \quad (13)$$

As concerns tr(J), according to condition (C.1) the trace of A is negative and $-k^2(D_{11}+D_{22})$ is

also negative. This leads to the fact that their sum, i.e. tr(J), is also negative. Therefore, Turing instability can occur only if det(J) < 0 for some value of k^2. To this aim, since $\det(\mathrm{D}) = D_{11}D_{22} - D_{12}D_{21} > 0$ (in order to have a dissipative diffusion coupling) and $\alpha\beta > 0$ (C.2), a first condition is $-\frac{\alpha}{2}D_{11} - 2D_{12} + \alpha\beta D_{21} > 0$. Then, in order to ensure the existence of a band of unstable spatial modes, the minimum of $\det(\mathrm{J})$ with respect to k^2 must be negative [17], leading to $\frac{\partial \det(J)}{\partial k^2} < 0$ which implies:

$$(-\frac{\alpha}{2}D_{11} - 2D_{12} + \alpha\beta D_{21})^2 - 8\det(D)\alpha\beta > 0 \tag{14}$$

It follows from the above analysis that the necessary conditions for system (6) to exhibit Turing patterns are

$$-\tfrac{\alpha}{2} < 0 \qquad (C.1)$$
$$\alpha\beta > 0 \qquad (C.2)$$
$$-\tfrac{\alpha}{2}D_{11} - 2D_{12} + \alpha\beta D_{21} > 0 > 0 \qquad (C.3)$$
$$(-\tfrac{\alpha}{2}D_{11} - 2D_{12} + \alpha\beta D_{21})^2 - 8\det(D)\alpha\beta > 0 \qquad (C.4)$$
$$\det(\mathrm{D}) = D_{11}D_{22} - D_{12}D_{21} > 0 \qquad (C.5)$$

We remark that, if only self-diffusions are present, i.e. $D_{12} = D_{21} = 0$, since D_{11} is a positive coefficient, conditions (C.1) and (C.3) cannot be simultaneously satisfied. Hence, in this case the instability must be driven by the cross-diffusion terms. So, at least $D_{21} \neq 0$ should be present allowing (C.1) to be satisfied.

4. Numerical results

Numerical simulations of the MCNN in Eqs. (6) have been performed considering $N = 100$. Without loss of generality, the initial conditions for the variables $x_{i,j}$ and $y_{i,j}$ have been drawn from a random uniform distribution between 0 and 1, and zero-flux boundary conditions are imposed. We consider the minimal case in which only the necessary cross-diffusion term D_{21} is present and check whether or not Turing Patterns emerge, therefore in the following we will consider $D_{12} = 0$.

We discuss now the numerical results obtained from the integration of the MCNN for a specific set of parameters, namely: $\alpha = 0.6$, $\beta = 1.5$, $D_{12} = 0$ and $D_{21} = 5$, $D_{11} = 5$, varying D_{22} to observe the different nature of the emerging patterns. In particular, diffusion coefficients affect the final state of the CNN, therefore, Turing pattern typology as a function of self-diffusion coefficients have been investigated. Different self-diffusion rates of the second variable, D_{22}, have been considered in our numerical simulations while keeping constant the left system parameters. As a result, different structures emerge as Fig. 2 shows. In particular, stripes (Fig. 2(a)), mixed (Fig. 2(b)) and spots (Fig. 2(c)) like patterns are obtained by only increasing D_{22} that assumes a value of $D_{22} = 2$, $D_{22} = 5$ and $D_{22} = 8$ respectively.

In Fig. 2, only layer x is shown; notice that the pattern is characterized by red structures in blue blackground. Below, we will discuss a case of a reverse pattern, with blue structures in a red balckground.

A broader investigation of the effects of both the self-diffusion coefficients on pattern selection has then been performed. In particular, in Fig. 3 a sketch of the different regions of the parameter space D_{11} and D_{22} is presented, when $\alpha = 0.6$, $\beta = 1.5$, $D_{12} = 0$, $D_{21} = 5$.

It is noteworthy that in Fig. 3 two mixed stripe/spot areas appear, one emerges between the spots domain area and the stripes one, while the other emerges between the stripes domain area and the unstable one. In particular, the latter mixed region for which D_{11} assumes higher values is characterized by a peculiar behavior. The emerging patterns have a reversed structure respects the ones previously shown in Fig. 2, i.e. the emerging patterns are characterized by blue stripes and spots in red background, Fig. 4.

The spatial wavelength of the emerging pattern has then been explored. The same topic has been investigated in [18], where the critical wave number at the onset of Turing patterns is defined as the degenerate root of $det(J)$ in (13). Thus, by solving this quadratic equation respect k^2, the roots are

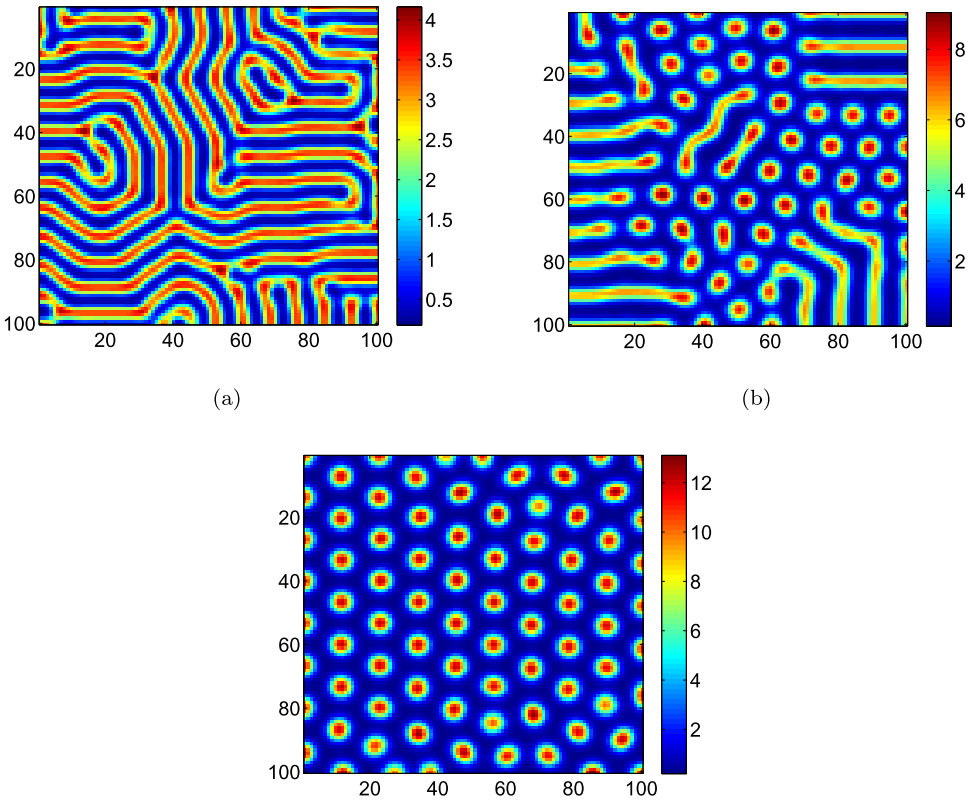

(a) (b)

(c)

Fig. 2. Turing patterns generated from a 100×100 MCNN as in Eqs. (6) in layer x, where D_{22} assumes three different values: (a) $D_{22} = 2$, stripes, (b) $D_{22} = 5$, mixture of stripes and spots, (c) $D_{22} = 8$, red spots in blue background. The other parameters are fixed as: $\alpha = 0.6$, $\beta = 1.5$, $D_{11} = 5$, $D_{12} = 0$, $D_{21} = 5$. Without loss of generality, initial conditions are taken randomly from a uniform distribution between 0 and 1, zero-flux boundary conditions are considered.

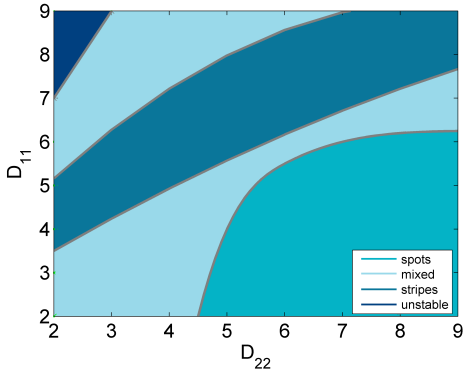

Fig. 3. Dependence of the type of pattern on the self-diffusion coefficients D_{11} and D_{22}. Other parameters are fixed as $\alpha = 0.6$, $\beta = 1.5$, $D_{12} = 0$, $D_{21} = 5$. Different colors indicate the emergence of stripes, spots, or mixed stripe/spot patterns.

$$k^2 = \frac{(\alpha\beta D_{21} - \frac{\alpha}{2} D_{11} - 2D_{12})}{2\det(D)} \pm \frac{\sqrt{(\alpha\beta D_{21} - \frac{\alpha}{2} D_{11} - 2D_{12})^2 - 4\det D}}{2\det(D)} \tag{15}$$

Roots will degenerate when condition the following condition holds:

$$(\alpha\beta D_{21} - \frac{\alpha}{2} D_{11} - 2D_{12})^2 = 4D_{11}D_{22} \tag{16}$$

By plugging (16) in (15), the critical wave number is derived as

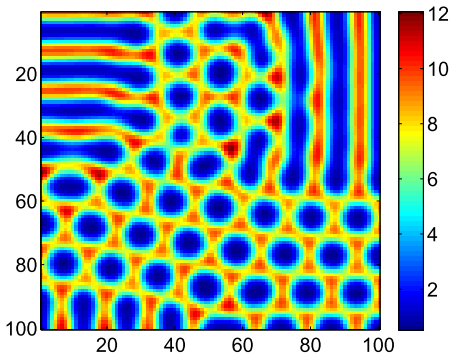

Fig. 4. Reverse mixed pattern when $D_{11} = 9$, $D_{12} = 0$, $D_{21} = 5$, $D_{22} = 6$, $\alpha = 0.6$, $\beta = 1.5$.

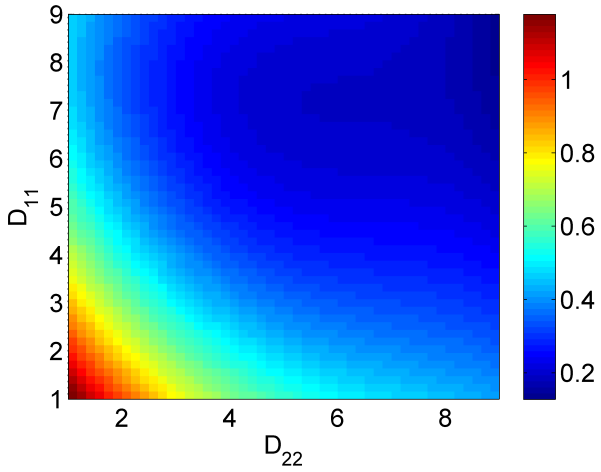

Fig. 5. Relationship between the pattern spatial frequency $k^2{}_c$ and the self-diffusion terms D_{11} and D_{22}.

$$k_c^2 = \sqrt{\frac{\det(\mathrm{A})}{\det(\mathrm{D})}} \tag{17}$$

Since the relationship between the wave number and the spatial wavelength is

$$\Omega = \frac{2\pi}{k_c} \tag{18}$$

it follows that

$$\Omega = \frac{2\pi}{k_c} = \frac{2\pi}{\sqrt{\frac{\det(A)}{\det(D)}}} \tag{19}$$

From Eqs. (17) and (19) it follows that patterns with different spatial wavelength may emerge by changing D_{11} and D_{22}. In particular, by increasing the product $D_{11}D_{22}$, the wave number decreases as it shown in Fig. 5 where k_c is mapped as a function of the self-diffusion coefficients. Patterns at different spatial frequency can be obtained by setting the parameters to $\alpha = 0.6$, $\beta = 1.5$, $D_{12} = 0$ and $D_{21} = 5$ and changing D_{11} and D_{22}: for lower values of D_{11} and D_{22}, higher wave numbers.

It can be noticed that for both the stripes (Figs. 6(a), 6(c)) and spots (Figs. 6(b), 6(d)) patterns, the spatial frequency decreases as $D_{11}D_{22}$ increases. It is important to remark that these values satisfy conditions (C.1)–(C.6).

5. Conclusions

The possibility to implement electronic devices able to reproduce complex spatio-temporal patterns is a well established result. This research aimed at reducing the complexity of the electronic device towards the simplest possible. Under this perspective, using a device incorporating a memristive element allowed us to reduce to only two components the topology of the basic unit.

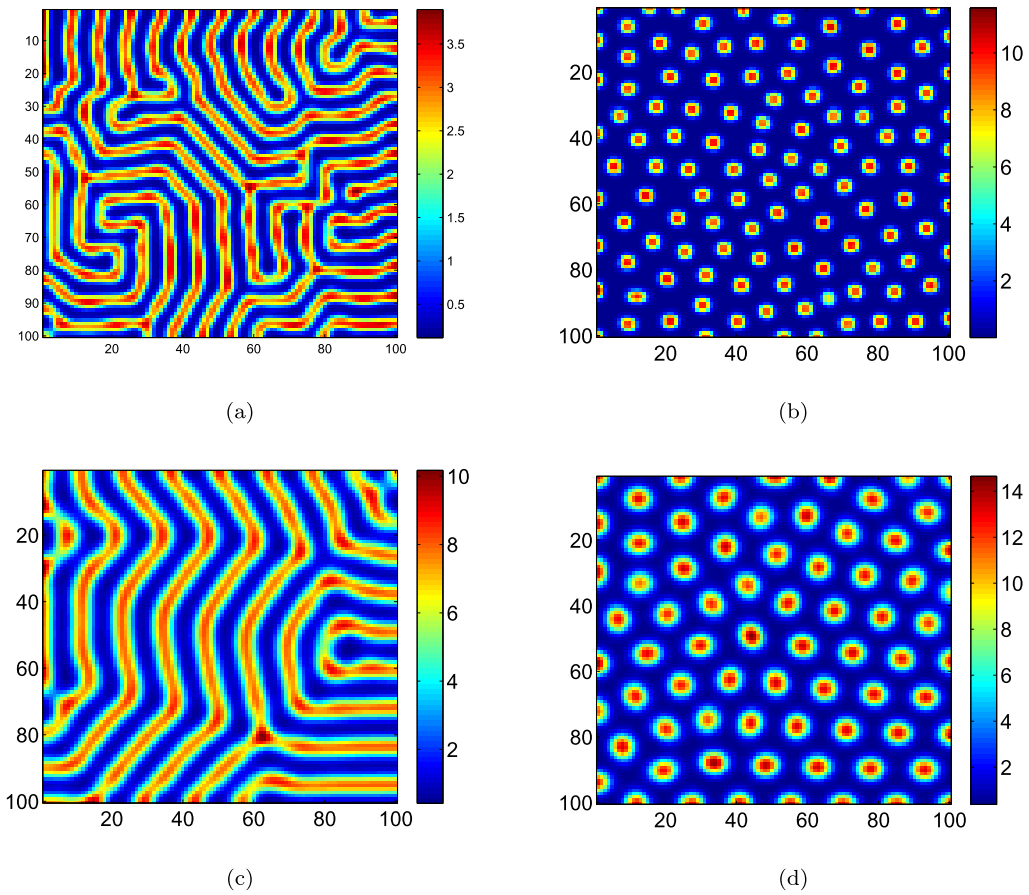

Fig. 6. Turing patterns generated from a 100×100 MCNN on layer x obtained (a–c) by fixing $D_{21} = 5$ and $D_{12} = 0$ and by varying D_{11} and D_{22}. (a) $D_{11} = 4$ and $D_{22} = 2$, (b) $D_{11} = 2$ and $D_{22} = 9$, (c) $D_{11} = 8$ and $D_{22} = 5$, (d) $D_{11} = 6$ and $D_{22} = 8$. Other parameters as indicated in the text.

We focused on Turing patterns and on deriving the conditions to design the memristive device able to show their emergence. By means of numerical simulations, different types of patterns, including spots, stripes, mixed and reverse conditions, have been obtained. Furthermore, the analysis of the spatial wavelength of the emerging patterns has been performed with respect to the parameters of the diffusion process. Interestingly, the simplicity of the cell leads to a simplification of the diffusion coupling mechanism needed to obtain Turing patterns. With reference to the results presented in [6], in which both variables undergo a cross-diffusion coupling, here we have found that a single cross-diffusion is sufficient to satisfy Turing conditions. From a modeling point of view, this result may represent a fundamental insight since the occurrence of a single cross-diffusion is typical of real phenomena such as pattern formation in chemotaxis and social systems [5].

In the perspective of real implementations of memristor-based systems generating Turing patterns, the simplicity of the cell here studied seems a particularly important factor. Another potential advantage could derive from the characteristics of the recently introduced $\Phi-$ memristor [19], a simple device accounting for a direct flux-charge interaction composed by a conductor carrying a controlled amount of current located in proximity to a magnetic lump and, simultaneously, sensing the possibly induced voltage by the switched flux. In particular, with such devices, the possibility of obtaining diffusion among the fluxes of memristive elements as a direct consequence of having adjacent memristors in concentrated circuits [20] can be explored. However, it remains to be solved the limitation that, currently, $\Phi-$ memristors are passive components.

Acknowledgments

This paper is supported in part by the EUROFUSION Consortium within the Contract of Association ENEA-UNICT and by University of Catania under the project “Piano della Ricerca 2016-18. Linea

intervento 2".

References

[1] A. Turing, "The chemical basis of morphogenesis," *Philosophical Transactions of the Royal Society of London B: Biological Sciences*, vol. 237, pp. 37–72, 1952.

[2] A.K. Harris, D. Stopak, and P. Warner, "Generation of spatially periodic patterns by a mechanical instability: A mechanical alternative to the Turing model," *Development*, vol. 80, no. 1, pp. 1–20, 1984.

[3] L. Goras and L.O. Chua, "Turing patterns in CNNs. II. Equations and behaviors," *IEEE Transactions on Circuits and Systems I: Fundamental Theory and Applications*, vol. 42, no. 10, pp. 612–626, 1995.

[4] U. Daybelge, C. Yarim, and A. Nicolai, "Spatiotemporal oscillations in tokamak edge layer and their generation by various mechanisms," 24th IAEA Fusion Energy Conf., 2012.

[5] V.K. Vanag and I.R. Epstein, "Cross-diffusion and pattern formation in reaction-difusion systems," *Physical Chemistry Chemical Physics*, vol. 11, no. 6, pp. 897–912, 2009.

[6] A. Buscarino, C. Corradino, L. Fortuna, M. Frasca, and L.O. Chua, "Turing patterns in memristive cellular nonlinear networks," *IEEE Transactions on Circuits and Systems I: Regular Papers*, vol. 63, no. 8, pp. 1222–1230, 2016.

[7] D.B. Strukov, G.S. Snider, D.R. Stewart, and R.S. Williams, "The missing memristor found," *Nature*, vol. 453, pp. 80–83, 2008.

[8] A. Ascoli, S. Slesazeck, H. Mahne, R. Tetzlaff, and T. Mikolajick, "Nonlinear dynamics of a locally-active memristor," *IEEE Transactions on Circuits and Systems I: Regular Papers*, vol. 62, no. 4, pp. 1165–1174, 2015.

[9] L.O. Chua, "Memristor—The missing circuit element," *IEEE Trans. Circuit Theory*, vol. 18, no. 5, pp. 507–519, 1971.

[10] M. Itoh and L.O. Chua, "Memristor oscillators," *International Journal of Bifurcation and Chaos*, vol. 18, no. 11, pp. 3183–3206, 2008.

[11] A. Buscarino, L. Fortuna, M. Frasca, and L.V. Gambuzza, "A chaotic circuit based on Hewlett-Packard memristor," *Chaos: An Interdisciplinary Journal of Nonlinear Science*, vol. 22, no. 2, 2012.

[12] A. Buscarino, L. Fortuna, M. Frasca, and L.V. Gambuzza, "A gallery of chaotic oscillators based on HP memristor," *International Journal of Bifurcation and Chaos*, vol. 23, no. 5, 2013.

[13] A. Buscarino, C. Corradino, L. Fortuna, M. Frasca, and L.O. Chua, "Evidence of Turing patterns in memristive Cellular Nonlinear Networks," CNNA 2016; 15th International Workshop on Cellular Nanoscale Networks and Their Applications, 2016.

[14] V.T. Pham, A. Buscarino, L. Fortuna, and M. Frasca, "Autowaves in memristive cellular neural networks," *International Journal of Bifurcation and Chaos*, vol. 22, no. 8, 1230027, 2012.

[15] B. Muthuswamy and L.O. Chua, "Simplest chaotic circuit," *International Journal of Bifurcation and Chaos*, vol. 20, no. 5, pp. 1567–1580, 2010.

[16] J.D. Murray, *Mathematical Biology. II Spatial Models and Biomedical Applications*, Springer-Verlag New York Incorporated, 2001.

[17] A. Madzvamuse, S.N. Hussaini, and R. Barreira, "Cross-diffusion-driven instability for reaction-diffusion systems: Analysis and simulations," *Journal of Mathematical Biology*, vol. 70, no. 4, pp. 709–743, 2015.

[18] Q. Ouyang, R. Li, and H.L. Swinney, "Dependence of Turing pattern wavelength on diffusion rate," *The Journal of Chemical Physics*, vol. 102, no. 6, pp. 2551–2555, 1995.

[19] F.Z. Wang, L. Li, L. Shi, H. Wu, and L.O. Chua, "Φ-memristor: Real memristor found," *Journal of Applied Physics*, vol. 125, no. 5, 054504, 2019.

[20] J.K. Eshraghian, H.H. Iu, T. Fernando, D. Yu, and Z. Li, "Modelling and characterization of dynamic behavior of coupled memristor circuits," *2016 IEEE International Symposium on Circuits and Systems (ISCAS)*, pp. 690–693, 2016.